Ophthalmic Application of Optical Coherence Tomography Angiography for Retina and Choroidal Imaging

Xiao Zhou

A thesis

submitted in partial fulfillment of the

requirements for the degree of

Master of Science in Bioengineering

University of Washington

2021

Committee:

Ruikang K. Wang

Kasra Rezaei

Program Authorized to Offer Degree:

Department of Bioengineering

University of Washington

Abstract

Ophthalmic Application of Optical Coherence Tomography Angiography for Retina and Choroidal Imaging

Xiao Zhou

Chair of the Supervisory Committee:

Professor Ruikang K. Wang

Bioengineering

Optical coherence tomography (OCT) angiography (OCTA) is a revolutionary non-invasive imaging modality that has been widely utilized in ophthalmology. OCT and OCTA has huge potentials for quantitative analysis based on its ability of detecting high-resolution three-dimensional data. In this thesis, the capacity of OCT detecting choroidal vasculature was demonstrated and techniques to quantify choroidal lesion character was described and showed advantages when compare to other imaging techniques. Also, vascular quantification tools for retina and choroidal microvasculature with different subregional analyze were proposed and tested on clinical OCTA system data of diseased subjects. Overall, the thesis presents a set of tools that can extract features from human ocular vasculature and generate regionally and quantitatively analysis.

TABLR OF CONTENTS

CHAPTER 1. INTRODUCTION **6**

1.1 Optical coherence tomography 7

1.2 Time domain optical coherence tomography 7

1.3 Fourier domain optical coherence tomography 8

1.3.1 Spectral domain optical coherence tomography *9*

1.3.2 Swept-source optical coherence tomography *10*

1.4 Optical coherence tomography angiography 11

CHAPTER 2. QUANTITATIVE ANALYSIS OF RETINA AND CHOROIDAL MICROVASCULATURE USING OPTICAL COHERENCE TOMOGRAPHY **12**

2.1 Introduction 12

2.2 Method 13

2.2.1 Retina vasculature quantification *13*

2.2.2 Choroidalcapillary flow deficits quantification in RPD *15*

2.3 Results 17

2.4 Discussion 18

CHAPTER 3. EN FACE AREA QUANTIFICATION OF CHORODIAL MASS LESIONS USING SWEPT SOURCE OPTICAL COHERENCE TOMOGRAPHY **19**

3.1 Introduction 19

3.2 Methods 21

3.2.1 Study Population *21*

3.2.2 Image Acquisition Choroidal Mass Lesion Segmentation and Quantification *21*

3.2.3 Clinical Image Assessment *23*

3.2.4 Statistical Analysis *24*

3.3 RESULTS 24

3.4 CONCLUSIONS 29

3.5 DISCUSSION 29

BIBLIOGRAPHY 31

Chapter 1. INTRODUCTION

Blindness and visual impairment have an important impact on our daily life, which can affect people's ability to perform everyday tasks and the interaction with others. In 2015, the world has been estimated that will have 36 million people under blind. 404 million people had varying degrees of visual impairment, 46% of them had mild visual impairment, over 50% had severe vision impairment.[1] In these people under visual impairment, it is possible to be prevented or treated for over 80% of them. World-widely, age-related macular degeneration, glaucoma, diabetic retinopathy, proliferate diabetic retinopathy, refractive errors and trachoma are the main reasons that causing vision impairment. And in the developing countries and low-income area, the leading causes of vision impairment are uncorrected refractive errors and cataract. In developed countries and high-income areas, the leading causes of vision impairment are retinal disease. According to the nation eye institute, there is an estimation that 4.2 million Americans have vision issues. 1.3 million of them are suffered from blind and 2.9 million of them have low vision and an estimated annual economic burden, $139 billion will be cost in USA in vision loss and eye diseases, also vision disorders.[2]

In clinical ophthalmology, it is significant to diagnose the vision disease in the early stage since the effectively early treatment can prevent some of the unnecessary irreversible damages which could be caused by the late treatment. There are several ophthalmic imaging techniques that has been developed in the world to help slit lamp microscope to help doctors to got accurate diagnosis in the early stage. Fluorescein angiography (FA) is a imaging technique that image the injected dye which can perform better visual information of blood vessel, thereby we can acquire nice retina vasculature visualization.[3] Indocyanine green angiography (ICGA) is really useful to image deep layer of eye, such as choroidal vasculature. This technique can absorb (805 nm) and

reflects (835 nm) the near infrared portion of the spectrum, which is helpful to visual choroidal neovascularization.[4] But even these two imaging techniques can provide vessel images, due to the injected dye and contrast agents are required before imaging, they could also cause life-threatening complications. [5] Ultrasonography is a non-invasive imaging technique, which have better depth of penetration, however, this technique cannot avoid directly contact with the eyeball and really have limited resolution that around 200 μm. [6]

1.1 Optical coherence tomography

Optical coherence tomography (OCT) is a revolutionary non-invasive optical imaging modality with depth-resolved volumetric information that has been widely utilized in ophthalmology. [7] OCT is a popular way in many filed of imaging, especially in ophthalmology because of nature. OCT fast imaging speed is up to 1.7MHz, high axial resolution is up to 1 μm and the imaging depth is around 3mm. [8–10] Low coherence interferometry is the basis of OCT, which demonstrate as the light from broad band light source that separate into reference arm and sample arm, and the light that travels from the refence arm will travel to the reference mirror and reflects back and then meet the light that reflected from sample in different depths. And after they meet and combine, an interference phenomenon will be appeared if the reference path length is equals to the sample arm length. Generally, there are two kinds of OCT, one is time domain OCT (TDOCT), and another is Fourier domain OCT (FDOCT)

1.2 Time domain optical coherence tomography

The very first version of OCT is time domain OCT. Figure 1.1 showed the time domain basic system. This system use a mechanically reference mirror to get depth-resolved imaging so that the scan speed is limited. With the speed of 2-8 kHz in the Aline scan, usually, TDOCT can only aimed to achieve 2 dimensional (2D) images of human eyes. Because it is hard to keep patient stay still for a long time to avoid the moving artifacts, the 3-dimensional (3D) imaging which need multiple 2D B-scans to generate a volume data is really a challenge.

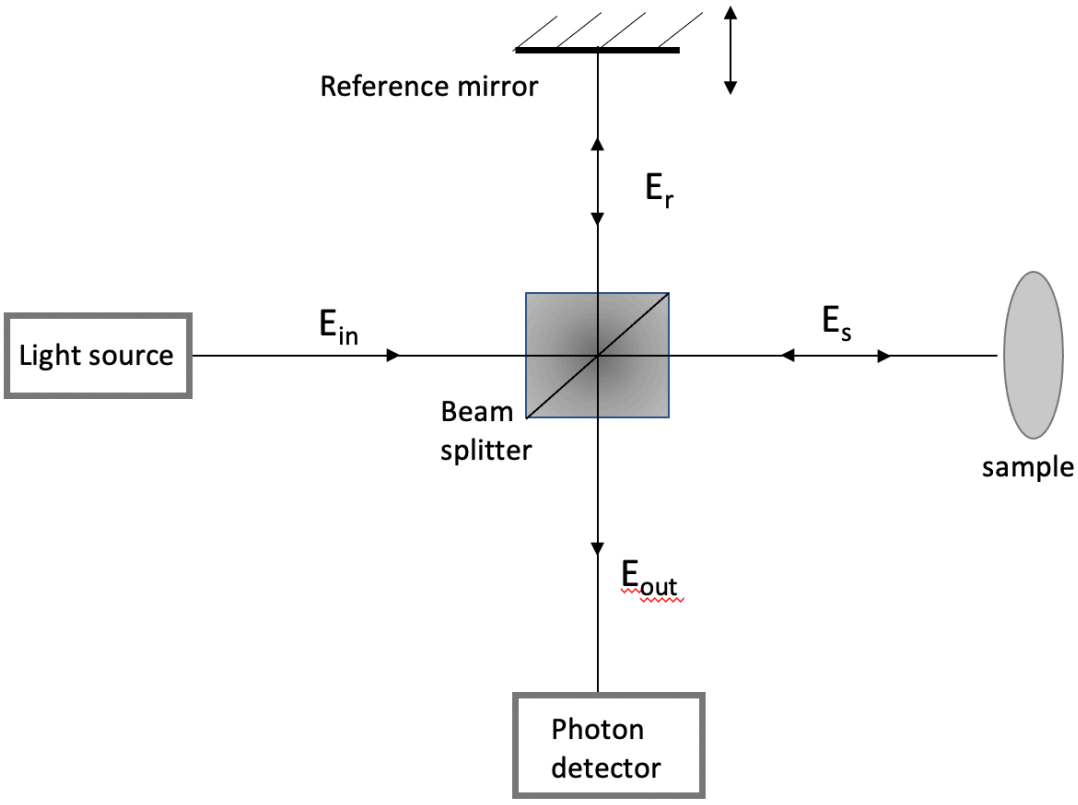

Figure 1.1 Schematic illustration of basic TDOCT set up

$\boldsymbol{E_{in}}$ incident light; $\boldsymbol{E_r}$ reference light; $\boldsymbol{E_s}$ sample light; $\boldsymbol{E_{out}}$ detected light.

1.3 Fourier domain optical coherence tomography

Fourier domain OCT is an OCT that have same principles as TDOCT. However, in FDOCT, the scanning mirror is been replaced of spectral interference which can get depth information, and then this spectral interference will be transfer and code as a function of the wavelength of light which is different to TDOCT that have scanning mirror to achieve the depth information in the sample by interference. The speed of A-line in FDOCT is significantly improved compare to TDOCT, so that the scanning data can be imaged with less motion artifacts. FDOCT can be divided into two different types based on the interferogram detection: spectral domain OCT (SDOCT) and swept-source OCT (SSOCT).

1.3.1 Spectral domain optical coherence tomography

Spectral domain OCT have a broadband light source and spectrometer, figure 1.2 illustrates the SDOCT system configuration. The interference that combined with two reflected light will be transfer to different wavelength components. The scanning camera will detect the combined interference and then transfer them into Fourier transform which could resolve the frequency corresponds to the depth and also the amplitude that correlate to the reflectivity. When applying a two dimensional scanner, the system can acquire the B-scan that been combined by the A-lines, and then these B-scans can be combined into a 3D dataset.

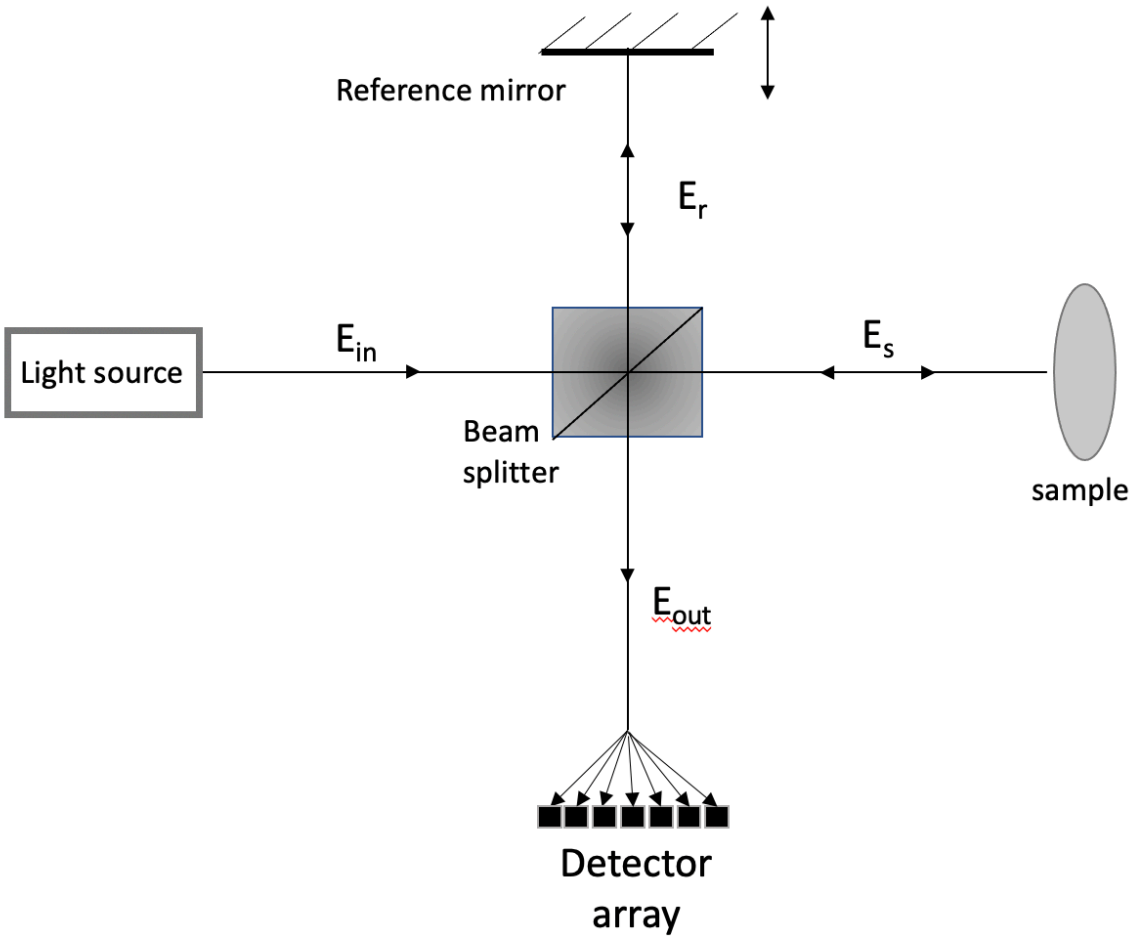

Figure 2.2 Schematic illustration of basic FDOCT set up

$\boldsymbol{E_{in}}$ incident light; $\boldsymbol{E_r}$ reference light; $\boldsymbol{E_s}$ sample light; $\boldsymbol{E_{out}}$ detected light.

1.3.2 Swept-source optical coherence tomography

Swept-source OCT generally takes Michelson interferometer as the main body, it uses a linear array camera to record the low coherence interference spectral signals of the broadband light source. And acquire parallelly of the depth information inside the sample. The imaging speed of this techniques mainly depends on the sweep frequency of the light source. Due to the

development of this high-speed scanning light source technology, the MHz scanning speed can be realized.

1.4 Optical coherence tomography angiography

OCT can also provide a depth-resolved 3D data with a new technique, angiography. The OCT 3D data we acquired from the biological sample is combined with static signals and moving signals. Every time we got multiple OCT scans that along different time points, we can acquire information from moving particles while the tissues are static. These differences from static tissues and moving particles can be used to analyzing in OCT signal variation along time. They can be categorized into different groups if they based on or use 1) phase part of OCT signal, 2) amplitude part of the signal or 3) whole complex OCT signal.

No matter which kind of OCTA system, they all have great potential in both research and clinical ophthalmology for various of ocular diseases. OCTA have several obvious advantages that make it such popular when compared to traditional dye-based angiography: 1) OCTA is non-invasive and safer, 2) OCTA can provide 3D date with detailed depth-resolved vasculature information, 3) OCTA have a high lat4ral resolution that can image capillaries. With these reasons, OCTA is more suitable than those dye-based angiographies, such as FA, ICGA and etc.

Chapter 2. QUANTITATIVE ANALYSIS OF RETINA AND CHOROIDAL MICROVASCULATURE USING OPTICAL COHERENCE TOMOGRAPHY

2.1 Introduction

Optical coherence tomography angiography was recently introduced for the image of microvasculature networks in the human eye.[11] Recent investigation using OCTA have been mainly focused on showing the application of visualization the flow characteristics of microvascular diseases with the macula.[12] When compare to traditional dye-based angiography, OCTA is safer and faster for macular vasculature imaging. Currently, OCT and OCTA can provide integrated structural and flow data in a non-invasive way and can also have the potential for quantitative analysis on complex vasculature. Optical microangiography (OMAG)[11] is one of OCTA approaches highlight the contrast among static tissues and moving particles. OMAG is able to provide OCTA better vascular connectivity and better signal to noise ratio, also OMAG is more sensitive to the capillary blood flow which can potentially value the investigation.[13] There are many studies have introduced vessel parameters to describe OCT angiograms. Such as vessel area density and vessel skeleton density, these parameters have been reported that are helpful when analyze some disease such as age-related macular disease and diabetic retinopathy.

Choroidcapillaries (CC) is a thin but dense vascular monolayer that beneath Bruch's membrane (BM) in the inner choroid.[14–16] Many studies have reported that the CC vasculature is quiet different morphological expression that in the submuscular region, there will be a dense honeycomb network of freely interconnected capillaries separated by septa.[17] In the equatorial

and peripheral regions, there will be polygonal lobular network. [17] So that, rather than quantify CC vasculature directly, it is a better way to segment the CC flow deficits (FDs).

In this study, we introduce a comprehensive method based on OMAG to do quantification analysis for OCTA retina images. We proposed to use several parameters to quantitatively describe the retina images: vessel area density (VAD), vessel skeleton density (VSD), vessel diameter index (VDI), vessel perimeter index (VPI) and vessel complexity index (CVI) as well as several masks to help regionally analysis: large vessel mask, quadrant mask, sector mask, annulus mask, Garway-Heath map mask. Also investigate the CC quantification segmentation on reticular pseudodrusen (RPD).

2.2 Method

2.2.1 Retina vasculature quantification

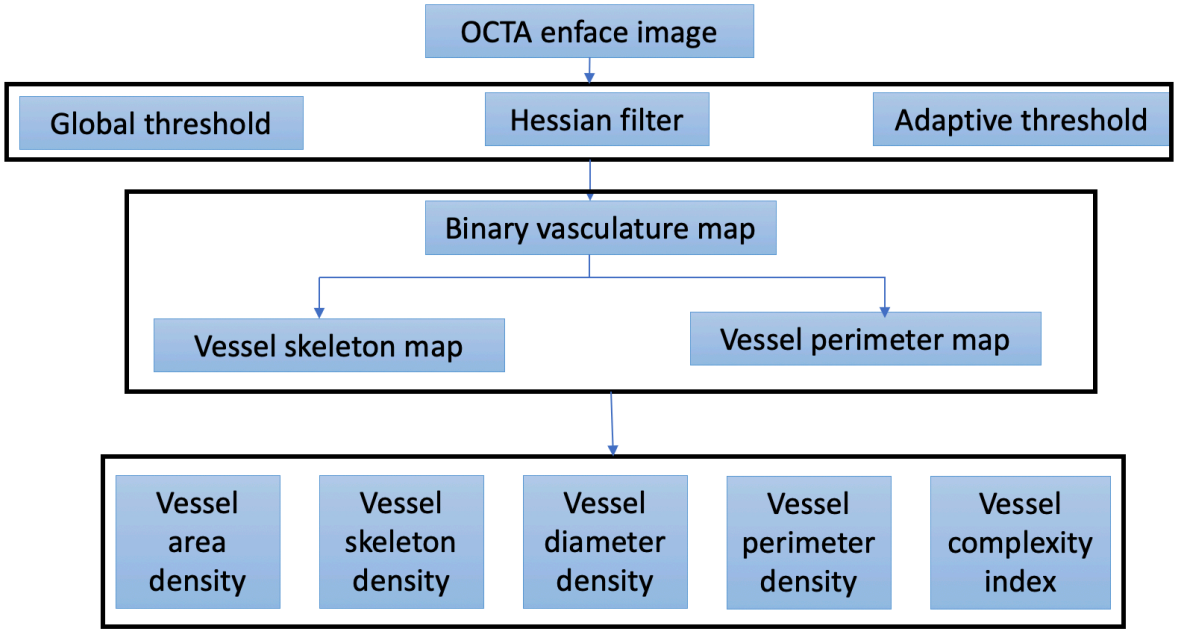

Figure 2.1. Overview of the quantitative OMAG algorithm.

OCTA imaging was performed using a 100-kHz SS-OCT PLEX Elite 9000 (Carl Zeiss Meditec, Dublin, California, USA), with a central wavelength of 1060 nm, a bandwidth of 100 nm, an axial resolution of ~6 μm, and a lateral resolution of ~ 20 μm estimated in retinal tissue.18 FastTrac (Carl Zeiss Meditec, Dublin, California) motion tracking was used during all scans to minimize possible motion artifacts. The complex optical microangiography (OMAGC) algorithm19 was used to generate OCTA volumes .The flowchart in Figure 2.1 is an overview of the processes involved in the quantitative method. The first step is generating a 2D enface image from 3D volume OCTA data (Figure 2.2A).

This image is processed into binary image in MATLAB R2019b software (Math Works, Natick, Massachusetts) using a global threshold, hessian filter,[18] and adaptive threshold. The global threshold is using one threshold parameter in foveal avascular zone by ask user to click specific place and generate noise floor. And then the hessian filter and adaptive threshold will be mixed and applied to a binary map. (Figure 2.2 B) After so, we can acquire the vessel area information, Next step is to get a skeletonized vessel map (Figure 2.2 C), in this map, all the vessels will be shrunk to a one-pixel line and the vessel length information can be acquired from this map. Last, we can generate vessel perimeter map from vessel area map by detect the edges of the vessels and acquire the vessel perimeter information.

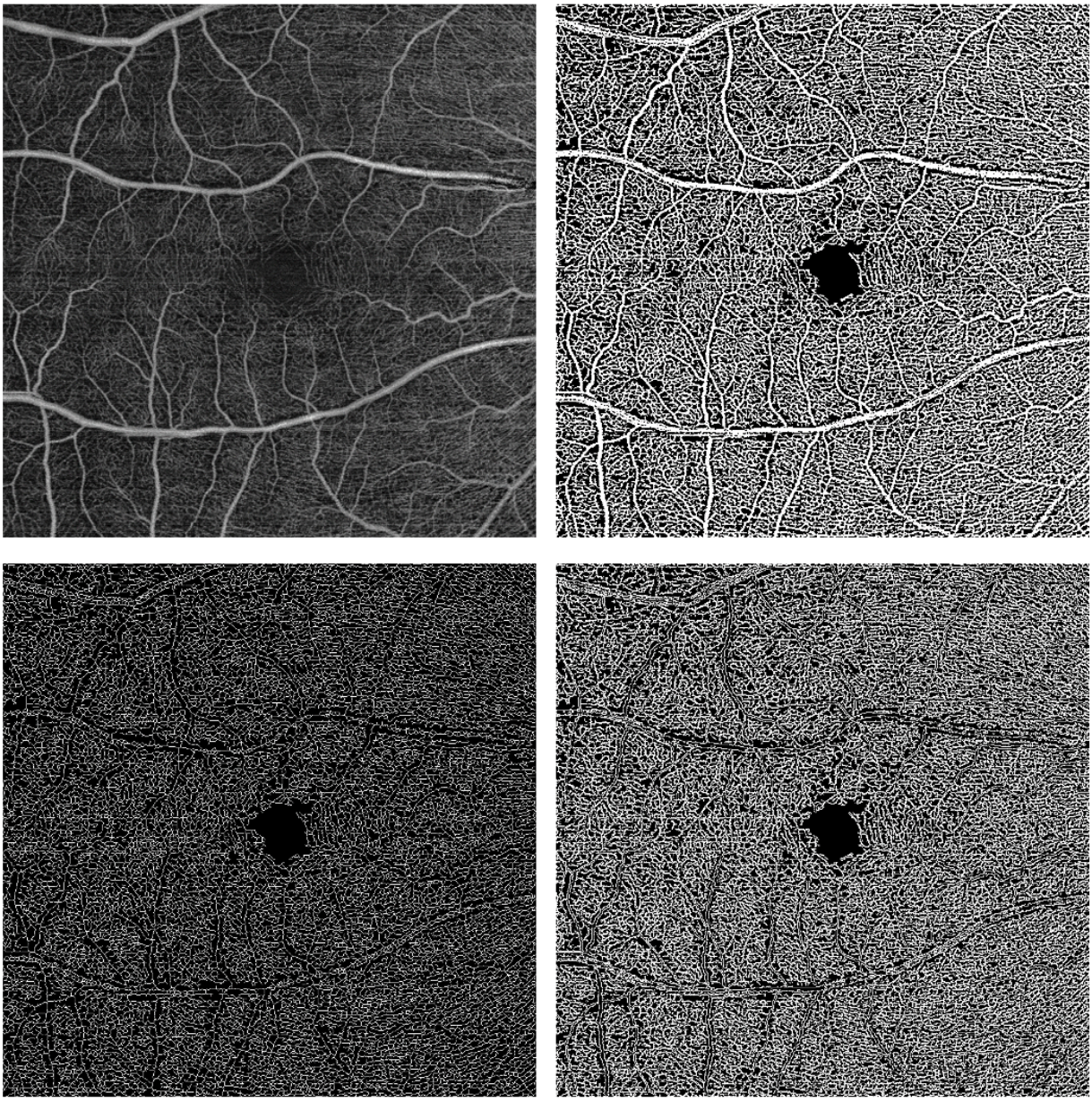

Figure 0.3. Representative OMAG images to illustrate the quantitative analysis algorithm.

(A) Original en face OMAG image. (B) Vessel area map (C) Vessel skeleton map (D)Vessel perimeter map

2.2.2 Choroidalcapillary flow deficits quantification in RPD

After acquiring volumetric SS-OCTA data, an automated algorithm was used to obtain accurate segmentation of BM layer, and all segmentation was reviewed and manually corrected

when necessary by one grader masked to diagnosis. The CC slab was defined as the region from 4μm to 20μm below the BM.[19] *En face* images were produced using a maximum projection method (Fig 2.3. A~B). A compensation strategy was applied to adjust for the signal attenuation due to drusen as previously described[20], retinal projection artifacts were subsequently removed[13] and corresponding regions were excluded in further analysis. The fuzzy C-means (FCM) method were used to segment flow deficits (FDs) in this study. This method automatically assigns all pixels in the entire image into different clusters based on histogram distribution.[21] The cluster with the lowest intensity is then segmented as the FDs. After thresholding, any FDs with an equivalent diameter smaller than the average normal intercapillary distance, 24 μm, were removed.[22] (Fig 2.3. E~F)

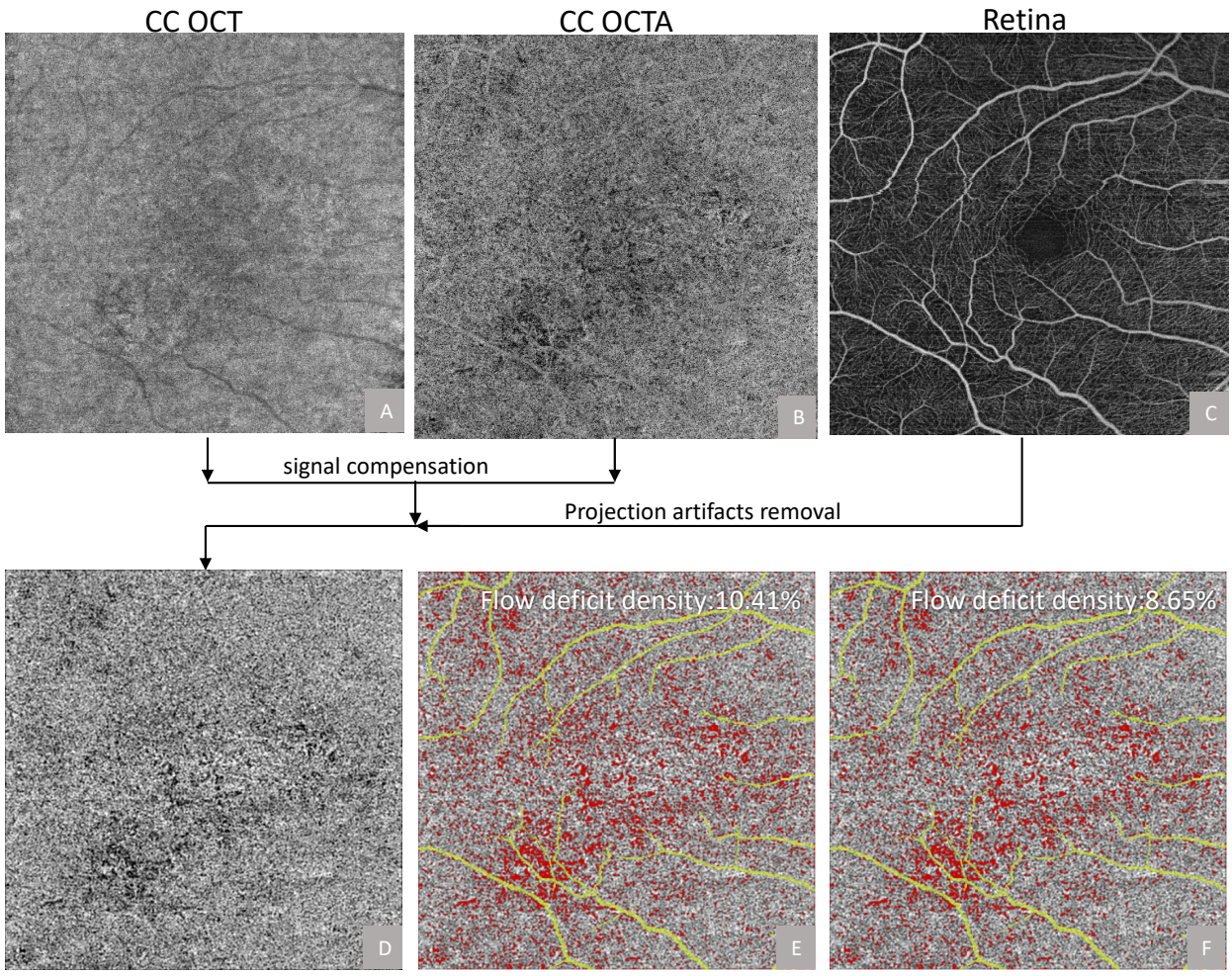

Figure 2.3 Choriocapillaris (CC) quantitative analysis using swept-source optical coherence tomography angiography (SS-OCTA). (A) the OCT CC en face image, generated by maximum projection. (B) the OCTA CC en face image, generated by maximum projection. (C) the OCTA retina en face image, generated by mean projection. (D) the OCTA CC en face image after signal compensation and projection artifacts removal. (E) Segmented flow deficits (FDs) (red) overlaid with the OCTA CC en face image(gray), retinal projections were excluded from analysis (yellow). (F) Segmented FDs map where FDs with an equivalent diameter smaller than 24 um (the normal inter-capillary distance) were removed.

2.3 Results

The three-dimensional nature of OCT allows for segmentation of vascular plex located at different physiological depths within the retina. We generated the retinal vasculature image from the internal limiting membrane to inner segment/ outer nuclear layer. This layer include ganglion cell layer, and the avascular outer retinal layer extending from outer nuclear layer to retinal pigment epithelium. With this algorithm, the VAD, VSD, VPI and VCI can be quantified from the processed images.

A total of 102 eyes from 51 participants were included in this study, and these participants were on average 73 ± 8 years old (range, 55 to 86 years old). A total of 47 (46%) eyes from 24 (47%) participants had definite RPD. Amongst the participants with definite RPD in either eye, 23 (96%) participants had bilateral definite RPD. The median drusen volume of all eyes was 0.08 mm3 (interquartile range [IQR] = 0.04 to 0.15 mm3). For the CC FD parameters, the median FD%, mean FD size and number of FDs were 8.3% (IQR = 7.1 to 8.9%), 1626 μm2 (IQR = 1532 to 1789 μm2) and 1684 (IQR = 1420 to 1841).

2.4 Discussion

In this report, there are five vessel parameters have been proposed, VAD, VSD, VDI, VPI and VCI. These parameters are used to do quantitative assessment on OCT angiograms. Several significant features are in this analysis approach. Vessel length, size, area, perimeter and the morphological complexity, these features are all can be used in a one-step imaging analysis which could potentially help the clinicians to have better understand OCTA images. Moreover, this quantitative algorithm can be multi used when try to select the region of interest. In this thesis, we mention a whole image processing and analysis, however, we can add more modules to make users select the part they are interested freely to do the OCT angiograms analysis.

There are several limitations as well. The first one is that OCTA data sometimes have projection artifacts from the large vessel in the superficial layer of retina which could affect the quality of enface image. In this way, these retube vasculature projected onto deeper layers of the retina are hard to notice only if the OCTA date can be segmented into superficial and deeper layer. Overall, this quantitative OCTA algorithm is really promising and have significant potential on clinical research.

Chapter 3. EN FACE AREA QUANTIFICATION OF CHORODIAL MASS LESIONS USING SWEPT SOURCE OPTICAL COHERENCE TOMOGRAPHY

3.1 Introduction

The differential diagnosis of a choroidal lesions is wide and includes benign, malignant, and inflammatory causes such as choroidal melanoma, choroidal nevus, choroidal hemangioma, metastatic tumors, and choroidal granulomas.[23] Determining the exact diagnosis can be difficult since biopsy is not feasible for most lesions due to their location and risk of ocular morbidity from this invasive procedure. For the majority of lesions, a combination of clinical exam and imaging findings are used to clarify the diagnosis.[23,24]

One important characteristic used to evaluate choroidal lesions is the size of the lesion. For example, the stable size of choroidal nevi can be used to help distinguish this benign lesion from a malignant choroidal melanoma.[25] If the lesion is malignant, an accurate determination of

size is also important in determining the risk of metastasis at the time of diagnosis, in deciding the most appropriate therapeutic option, and providing prognosis on vision after treatment.

The size of a choroidal lesion is currently determined by clinical exam or using ultrasonography. Measurements made on clinical exam use the optic nerve as a reference for size and describe the lesion area in units of "disc diameters" or disc areas. This measurement can be made by ophthalmoscopy or op color fundus images. While this is the most common form of measurement, the accuracy and reproducibility provided by this method is low due to the poor resolution.[26] Further complicating this form of measurement, when the choroidal lesion is not pigmented or is obscured by subretinal fluid the size and boundary in relationship to important places like the fovea and optic nerve can be even more challenging to determine.

Ultrasonography is another method that can be used to measure the height and base area of a choroidal lesion. However, ultrasonography has limited ability to resolve base boundaries from normal choroid when the lesion has a similar internal reflectivity, and can only provide measurements in millimeter increments with any accuracy [27,28]. Thus ultrasonography is not an idea tool for accurate measurement and long-term tracking and monitoring.

SS-OCT has the potential to improve the accuracy of choroidal lesion size measurements due to the ability of long wavelength light (1060 nm) used in SS-OCT imaging to penetrate below the RPE and the density of A-scans used to capture volume scans. Theoretically, SS-OCT imaging would allow for detection of changes in choroidal lesion size in the micron range rather than the mm range with the bandwidth of 100nm, we have the axial resolution of ~6 μm and the lateral resolution of ~ 20 μm.[29] Therefore, our study aimed to explore the potential in quantitatively analyze choroidal lesion size by measuring choroidal lesion area using SS-OCT.

3.2 Methods

3.2.1 Study Population

This single-institution retrospective observational study was approved by the Institutional Review Board at the University of Washington. Written informed consent regarding the nature of this research study was obtained for all subjects before imaging. This study was performed in accordance with the tenets of the Declaration of Helsinki and the Health Insurance Portability and Accountability Act of 1996.

Patients 19 years or older, with diagnosis of choroidal melanoma, choroidal hemangioma and choroidal nevus were recruited for SS-OCT imaging between September 2017 to March 2019 at the University of Washington Harborview Medical Center Eye institute. (Upon entry in the study, subject data including sex, age, disease diagnosis and were collected.) All patients underwent detailed clinical examination including fundus photography, fluorescein angiography, B-scan ultrasonography and optical coherence tomography. The diagnosis and classification of choroidal lesions was made by an ocular oncology trained subspecialist (A.S) after complete ophthalmic examination and review of clinically indicated imaging and laboratory studies.

3.2.2 Image Acquisition Choroidal Mass Lesion Segmentation and Quantification

OCT imaging was performed using a 100-kHz SS-OCT PLEX Elite 9000 (Carl Zeiss Meditec, Dublin, California, USA), with a central wavelength of 1060 nm, a bandwidth of 100 nm, an axial resolution of ~6 μm, and a lateral resolution of ~ 20 μm estimated in retinal tissue.[29] FastTrac (Carl Zeiss Meditec, Dublin, California) motion tracking was used during all scans to minimize possible motion artifacts. Montage Angio scanning protocol was selected with either 12x12 mm (5-scan composite) or 15x9 mm (2-scan composite) for both eyes of each subject to

obtain wide-field images containing the choroidal lesion. Five 12x12 mm scans (1= central macula, 2= superior nasal , 3 = inferior nasal, 4= superior temporal, and 5= inferior temporal) were obtained in an overlapping montage scanning pattern (Figure 3.1,A); two scans of 15x9 mm areas (superior, and inferior) were obtained in a 15x9 mm montage scanning pattern.[30] Single scans that contained the whole choroidal tumor were selected for further analysis (Figure 3.1,B), if the tumor was not contained entirely within one scans, all scans containing the tumor were montaged by an intensity based method prior for further analysis.

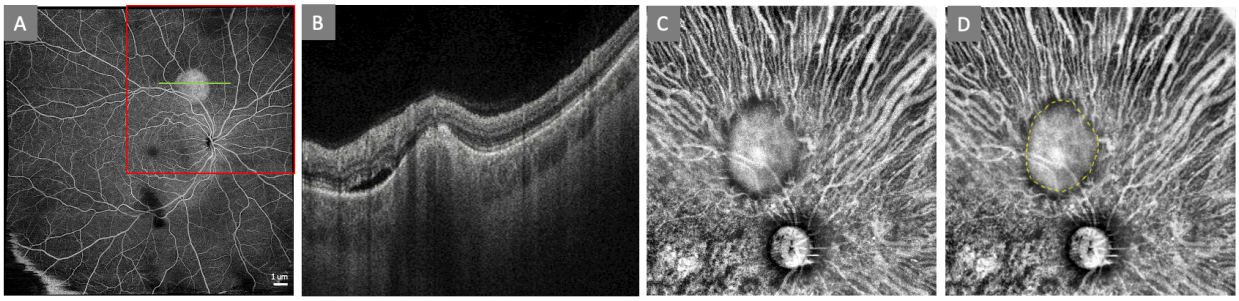

Figure 3.1 An eye with choroidal melanoma imaged by swept-source optical coherence tomography angiography(SS-OCTA): Wide-field image produced by montaging five overlapping 12x12 mm OCT scans. Red box indicates the area of the superior nasal scan that completely encompassed the choroidal lesion. B. B scan (green line in A) through the choroidal lesion demonstrates a domed lesion with homogenous reflectivity and associated subretinal fluid. C: Choroidal en face image demonstrates areas of normal choroidal vascular surrounding the choroidal lesion which demonstrates a homogenous pattern. E: Boundary of choroidal lesion demarcated with a dashed yellow line.

From the structure volume scans, the choroidal slab was defined as the region spanning from the retinal pigment epithelium (RPE)/Bruch's membrane (BM) complex layer to the outer boundary of the choroidal-scleral interface. After obtaining OCT volumes, attenuation correction

was performed as previously described[31] the choroidal slab was automatically segmented using the commercially available factory settings. All segmentations were reviewed by one author (XZ) and manual corrections performed when necessary[31]. Minimum projection was then applied to segmented choroidal slabs to generate choroidal vasculature en face images.

Manual delineation of the choroidal lesion was then performed by outlining the area of abnormal choroidal vasculature pattern (Figure 3.1, D).[32] Choroidal lesion area was defined on each enface image as the whole area inside the manual delineated lesion boundary. Maximum vertical inner diameter was defined as the maximum distance between the antipodal intersections of a vertical line and the boundary; Maximum horizontal inner diameter was defined as the maximum distance between the antipodal intersections of a horizontal line and the boundary.

3.2.3 Clinical Image Assessment

Clinical measurements of en face lesion area were made by the examining clinician and recorded in the clinical chart at the time of exam. After chart-based data extraction, any lesion that lacked measurements were noted. Clinical photos of the lesions obtained on the same day as the SS-OCTA were then presented to the examining physician and en face lesion area measurements were made per standard practice and this area was recorded. Clinical measurements were recorded in disk diameters (DD). DD was then converted micrometers using 1 DD = 1.5 μm. Ultrasound (US) B scan measurements were obtained by the examining physician (AS) or trained ophthalmic imaging technician by standard protocol. In brief, the tumor was identified using a ultrasound with phase probe. On transverse scans, images were captured, and the base measure by training physician. In brief, the tumor was identified using ultrasounds with probe. On transverse scans, images were captured, and the base measured

using. En face lesion area was approximated from B scan images by using the maximum base longitudinal and transverse length as the input for calculation of an ellipse.

3.2.4 Statistical Analysis

Statistical analysis was performed using MATLAB R2019b software (Math Works, Natick, Massachusetts) and R (R Foundation for Statistical Computing, Vienna, Austria). Intraclass correlation coefficient (ICC) Spearman correlation test was performed to determine the correlation between parameters. A value of ICC less than 0.5 was considered as poor agreement; a value of ICC more than 0.5 and less than 0.9 was considered as moderate agreement; a value of ICC more than 0.9 was considered as excellent agreement, Spearman correlation matrix were performed using custom R scripts.

3.3 Results

25 subjects with the diagnosis of "choroidal lesion" were identified from a centralized SS-OCT database and screened. Eyes were excluded if SS-OCT imaging was not performed within 3 months' time frame of the clinical measurements, (n=8) or if the lesion extended beyond the border of SS-OCT imaging window (n=3). Thus, the final study group consisted of 14 eyes from 14 subjects (Table 1). Five subjects (43%) with the diagnosis of melanoma, three (21%) with choroidal nevus, and five (36%) with choroidal hemangioma. The clinical record for each subject was reviewed and data extracted including specific diagnosis, clinical measurement of en face lesion area, and lesion measurements obtained using Ultrasound imaging. All eyes had SS-OCT imaging and clinical measurements obtained on the day of exam or upon follow up review

with the examining physician. Only 4 eyes had ultrasound measurements of the lesion performed on the same day or within 3 months of the SS-OCT images.

Table 3.1 Choroidal lesions included in the study and same day en face area measurements**.**

	Patient		Lesion			
No.	**Age**	**Gender**	**Diagnosis**	**SS-OCT measurement**	**Clinical measurment**	**US measurement**
1	53	F	Melanoma	18.65	21.21	-
2	78	M	Nevus	13.88	10.60	-
3	41	F	Hemangioma	20.22	9.42	-
4	38	M	Hemangioma	15.88	15.90	61.51
5	73	M	Hemangioma	10.23	44.18	59.80
6	62	M	Hemangioma	10.55	28.27	74.50
7	74	F	Melanoma	52.00	15.90	-
8	73	F	Melanoma	17.21	12.57	19.46
9	51	M	Melanoma	12.78	10.60	15.39
10	58	M	Melanoma	8.52	12.57	-
11	74	F	Nevus	32.89	35.34	38.41
12	54	F	Melanoma	56.73	44.16	-
13	65	F	Hemangioma	53.82	15.90	58.67
14	20	F	Nevus	8.18	7.07	-

SS-OCT was obtained on each lesion, the en face choroidal slab was generated, and lesion area measured manually (Figure 3.1). In en face images, normal choroidal vasculature is characterized by a homogeneous reticular pattern.[32] In contrast, in the area occupied by the choroidal lesion, the reticular vascular pattern is lost and demonstrates a more homogenous pattern (Figure 3.1C).

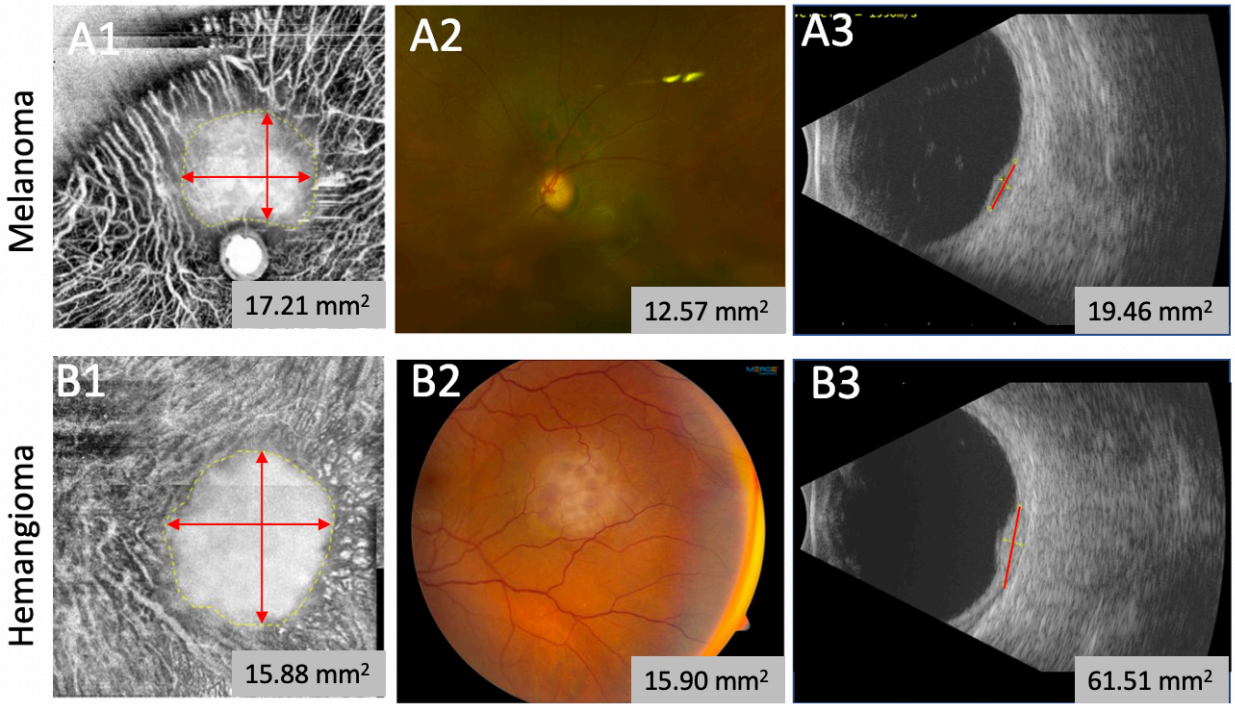

Figure 3.2 En face SS-OCT image of a choroidal melanoma with lesion boundary depicted as the yellow dash line and maximum horizontal and trasverse inner diameter depicted as red arrow line (A1) or hemangioma (B1). A2, B2: Color fundus. A3, B3: Ultrasound B-scan with base measurement in red.

Two examples comparing the color fundus imaging and ultrasound images to the en face image obtained by SS-OCT are shown in Figure 3.2. The choroidal melanoma in shown in Figure 3.2A is located immediately adjacent to the optic nerve at 12 o'clock and forms a focal elevation of the choroid seen on ultrasound in Figure 3.2 A, C. In the en face OCT image, the lesion appears as a white area with loss of the normal choroidal vasculature present adjacent to the optic nerve at 12 o'clock. Panel B compares the images obtained on a choroidal hemangioma. The color fundus shows an elevated hypopigmented lesion in the temporal macula. The ultrasound B-scan also show an elevated mass originating from the choroid. In the en face OCT image, the lesion appears as a sharply demarcated area with complete loss of the normal

choroidal vasculature pattern. Using each imaging modality, the en face area of the lesion was calculated and displayed in mm^2. For the melanoma and nevi, the OCT measurements were similar to the measurements made by clinical exam and US. For the hemangioma the OCT measurements were different to the measurements made by clinical exam and US.

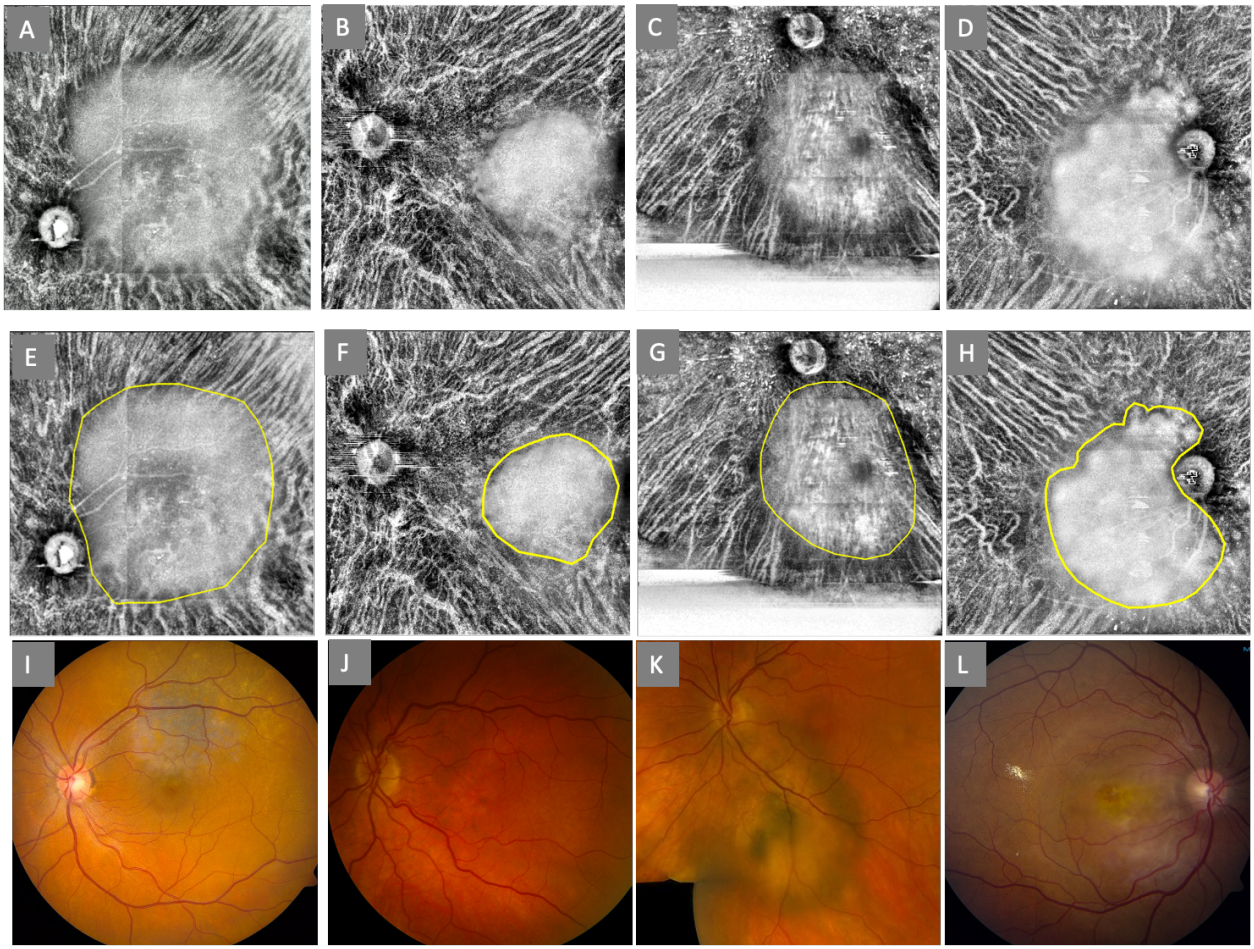

Figure 3.3 A-D: OCT en face images showing normal choroidal vasculature in homogeneous reticular pattern and choroidal bulging in a complete blurred patch; E-H: custom en face images showing choroidal mass lesion boundary on A-B by human grader depicted as the yellow dash line separately. I-L: color fundus images.

Figure 3.3 shows the en face OCT image from additional lesions. The type of lesion and the en face area measured by OCT are indicated on each image. For all lesions, the loss of

normal choroidal vascular pattern is visible, but there were differences in the borders and homogeneity of the lesions. Lesion A~D melanoma and nevi cases in figure 33. has a black border around the choroidal lesion compare to lesion E, F hemangioma cases. In different choroidal mass lesions (Figure 3.3, A~D), the normal structural choroidal vasculature is characterized by a homogeneous reticular pattern, and choroidal bulging is characterized as a complete blurred patch. Manual delineation of choroidal mass lesion was identified by the line of morphological demarcation on each subject. (Figure 3.3, E~H)

Finally, to determine if the en face lesion areas determined by OCT agreed with the measurements obtained by clinical exam and US, ICC Spearman correlation test was performed. (Figure 3.4) The agreement between OCT and fundus exam area was poor (ICC = 0.32). The agreement between US and fundus exam was moderate (ICC = 0.63). The agreement between US and OCT on the 4 lesions with same day imaging was excellent (ICC= 0.99).

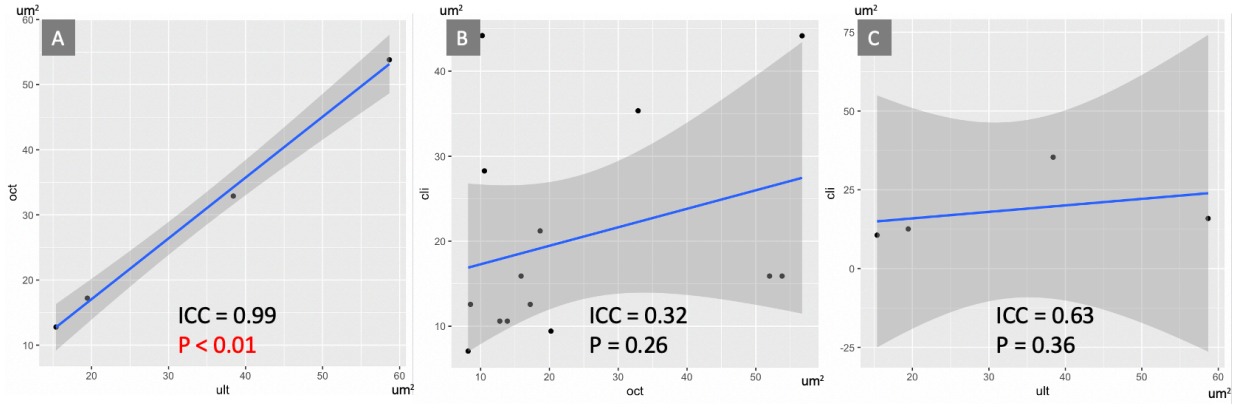

Figure 3.4 Agreement in enface lesion area between OCT and US (A), OCT and fundus exam (B), or US and fundus exam (C).

3.4 Conclusions

Pigmented and amelanotic fundus lesions can be identified in the SS-OCT choroidal en face projection. The resulting image provides a new method for lesion area measurement with excellent agreement to US measurements and could be useful for longitudinal monitoring. Larger studies with same day exam, SS-OCT, and ultrasound measurements will be required to verify the extent of agreement suggested by this pilot study.

3.5 Discussion

The study demonstrates the choroidal mass lesion area measurement have excellent correlation between ancillary technical: SS-OCT choroidal enface measurement and US measurement, and worse correlation between clinical examination measurement and ancillary technical. This result might suggest that measurement of choroidal mass lesion by SS-OCT enface is a diagnosis way as reliable as US measurement, which is widely used in quantify and diagnosis intraocular tumor[33–35], could potentially use for lesion area tracking and apply on monitoring recurrence of such disease.

Three lesions with mixed pigmentary components measured much smaller by fundus exam than by OCT or US.

The limitations of the current study is that the size measurement of choroidal mass lesion is been constrained by the ability of OCT, however, the montage scan protocol (over 12x12mm) in the SS-OCT used in this study is able to scan most choroidal tumors[36]. Also, the area measurement is not able to apply on the choroidal lesion like choroidal lymphoma, these lesion are diffused distribution and hard to be measured in area with a specific shape[37]. The other

limitation is a small sample size of 21 eyes, however, with a large sample size, it may be possible to reinforce the correlation between the OCT measurement and US measurement due to the present excellent agreement.

Further research is needed to improve the lesion measurement by an automatically way which could decrease the deviation of manual measurement. Also, the quantitative parameters include choroidal mass lesion volume and height may potentially benefit for disease diagnosis and tracking.

Bibliography

1. Bourne RRA, Flaxman SR, Braithwaite T, et al. Magnitude, temporal trends, and projections of the global prevalence of blindness and distance and near vision impairment: a systematic review and meta-analysis. *Lancet Glob Heal*. Published online 2017. doi:10.1016/S2214-109X(17)30293-0
2. AAO. US Eye Disease Statistics.
3. Rabb MF, Burton TC, Schatz H, Yannuzzi LA. Fluorescein angiography of the fundus: A schematic approach to interpretation. *Surv Ophthalmol*. Published online 1978. doi:10.1016/0039-6257(78)90134-0
4. Slakter J. Indocyanine-green angiography. *Curr Opin Ophthalmol*. 1996;(6(3)):P. 25-32.
5. Yannuzzi LA, Rohrer KT, Tindel LJ, et al. Fluorescein Angiography Complication Survey. *Ophthalmology*. Published online 1986. doi:10.1016/S0161-6420(86)33697-2
6. Bushberg JT. The Essential Physics of Medical Imaging, Third Edition. *Med Phys*. Published online 2013.
7. Pavlin CJ, McWhae JA, McGowan HD, Foster FS. Ultrasound Biomicroscopy of Anterior Segment Tumors. *Ophthalmology*. Published online 1992. doi:10.1016/S0161-6420(92)31820-2
8. Huang D, Swanson EA, Lin CP, et al. Optical coherence tomography. *Science (80-)*. Published online 1991. doi:10.1126/science.1957169
9. Cui D, Liu X, Zhang J, et al. Dual spectrometer system with spectral compounding for 1-μm optical coherence tomography in vivo. *Opt Lett*. Published online 2014. doi:10.1364/ol.39.006727
10. Gorczynska I, Migacz J V., Jonnal R, Zawadzki RJ, Poddar R, Werner JS. Imaging of the

human choroid with a 1.7 MHz A-scan rate FDML swept source OCT system. In: *Ophthalmic Technologies XXVII*. ; 2017. doi:10.1117/12.2251704

11. Wang RK, Jacques SL, Ma Z, Hurst S, Hanson SR, Gruber A. Three dimensional optical angiography. *Opt Express*. Published online 2007. doi:10.1364/oe.15.004083
12. Moult E, Choi W, Waheed NK, et al. Ultrahigh-speed swept-source OCT angiography in exudative AMD. *Ophthalmic Surg Lasers Imaging Retin*. Published online 2014. doi:10.3928/23258160-20141118-03
13. Zhang A, Zhang Q, Wang RK. Minimizing projection artifacts for accurate presentation of choroidal neovascularization in OCT micro-angiography. *Biomed Opt Express*. Published online 2015. doi:10.1364/boe.6.004130
14. Cao J, McLeod DS, Merges CA, Lutty GA. Choriocapillaris degeneration and related pathologic changes in human diabetic eyes. *Arch Ophthalmol*. Published online 1998. doi:10.1001/archopht.116.5.589
15. Lutty G, Grunwald J, Majji AB, Uyama M, Yoneya S. Changes in choriocapillaris and retinal pigment epithelium in age-related macular degeneration. *Mol Vis*. Published online 1999.
16. Bhutto I, Lutty G. Understanding age-related macular degeneration (AMD): Relationships between the photoreceptor/retinal pigment epithelium/Bruch's membrane/choriocapillaris complex. *Mol Aspects Med*. Published online 2012. doi:10.1016/j.mam.2012.04.005
17. Olver JM. Functional anatomy of the choroidal circulation: Methyl methacrylate casting of human choroid. *Eye*. Published online 1990. doi:10.1038/eye.1990.38
18. Frangi A, Niessen W, Vincken K, Viergever M. Multiscale vessel enhancement filtering Medical Image Computing and Computer-Assisted Interventation — MICCAI'98. In:

Medical Image Computing and Computer-Assisted Intervention — MICCAI'98. ; 1998.

19. Chu Z, Gregori G, Rosenfeld PJ, Wang RK. Quantification of Choriocapillaris with Optical Coherence Tomography Angiography: A Comparison Study. *Am J Ophthalmol*. Published online 2019. doi:10.1016/j.ajo.2019.07.003
20. Zhang Q, Zheng F, Motulsky EH, et al. A novel strategy for quantifying choriocapillaris flow voids using swept-source OCT angiography. *Investig Ophthalmol Vis Sci*. Published online 2018. doi:10.1167/iovs.17-22953
21. Chu Z, Zhang Q, Zhou H, et al. Quantifying choriocapillaris flow deficits using global and localized thresholding methods: a correlation study. *Quant Imaging Med Surg*. Published online 2018. doi:10.21037/qims.2018.12.09
22. Zhang Q, Shi Y, Zhou H, et al. Accurate estimation of choriocapillaris flow deficits beyond normal intercapillary spacing with swept source OCT angiography. *Quant Imaging Med Surg*. Published online 2018. doi:10.21037/qims.2018.08.10
23. Konstantinidis L, Damato B. Intraocular metastases - A review. *Asia-Pacific J Ophthalmol*. Published online 2017. doi:10.22608/APO.201712
24. De Jong MC, Van Der Meer FJS, Göricke SL, et al. Diagnostic accuracy of intraocular tumor size measured with MR imaging in the prediction of postlaminar optic nerve invasion and massive choroidal invasion of retinoblastoma. *Radiology*. Published online 2016. doi:10.1148/radiol.2015151213
25. Albert C, Scott I, Murray T, Shields C. Distinguishing a Choroidal Nevus From a Choroidal Melanoma. *OPHTHALMIC PEARLS*. Published online February 2012:40. https://www.aao.org/eyenet/article/distinguishing-choroidal-nevus-from-choroidal-mela
26. Ishibazawa A, Nagaoka T, Takahashi A, et al. Optical coherence tomography angiography

in diabetic retinopathy: A prospective pilot study. *Am J Ophthalmol*. Published online 2015. doi:10.1016/j.ajo.2015.04.021

27. Schuetzenberger K, Pfister M, Messner A, et al. Comparison of optical coherence tomography and high frequency ultrasound imaging in mice for the assessment of skin morphology and intradermal volumes. *Sci Rep*. Published online 2019. doi:10.1038/s41598-019-50104-4

28. Romero JM, Finger PT, Rosen RB, Iezzi R. Three-dimensional ultrasound for the measurement of choroidal melanomas. *Arch Ophthalmol*. Published online 2001. doi:10.1001/archopht.119.9.1275

29. Meditec CZ. Carl Zeiss Meditec Plex Elite 9000 OCT 501(k) premarket report of FDA. Published 2016. Accessed August 2, 2020. https://www.zeiss.com/meditec/int/product-portfolio/optical-coherence-tomography/plex-elite-9000-swept-source-oct.html#specifications

30. Meditec CZ. Plex® Elite 9000 Version 1.7 Instrctions for Use.

31. Zhou H, Chu Z, Zhang Q, et al. Attenuation correction assisted automatic segmentation for assessing choroidal thickness and vasculature with swept-source OCT. *Biomed Opt Express*. Published online 2018. doi:10.1364/boe.9.006067

32. Ferrara D, Waheed NK, Duker JS. Investigating the choriocapillaris and choroidal vasculature with new optical coherence tomography technologies. *Prog Retin Eye Res*. Published online 2016. doi:10.1016/j.preteyeres.2015.10.002

33. Dunavoelgyi R, Dieckmann K, Gleiss A, et al. Local tumor control, visual acuity, and survival after hypofractionated stereotactic photon radiotherapy of choroidal melanoma in 212 patients treated between 1997 and 2007. *Int J Radiat Oncol Biol Phys*. Published

online 2011. doi:10.1016/j.ijrobp.2010.04.035

34. Finger PT, Chin KJ, Duvall G. Palladium-103 Ophthalmic Plaque Radiation Therapy for Choroidal Melanoma: 400 Treated Patients. *Ophthalmology*. Published online 2009. doi:10.1016/j.ophtha.2008.12.027

35. Barbazetto I, Schmidt-Erfurth U. Photodynamic therapy of choroidal hemangioma: Two case reports. *Graefe's Arch Clin Exp Ophthalmol*. Published online 2000. doi:10.1007/s004170050346

36. Shields CL, Furuta M, Thangappan A, et al. Metastasis of uveal melanoma millimeter-by-millimeter in 8033 consecutive eyes. *Arch Ophthalmol*. Published online 2009. doi:10.1001/archophthalmol.2009.208

37. Mashayekhi A, Shukla SY, Shields JA, Shields CL. Choroidal lymphoma: Clinical features and association with systemic lymphoma. *Ophthalmology*. Published online 2014. doi:10.1016/j.ophtha.2013.06.046